Abstract

The two-photon reaction $\gamma\gamma \rightarrow \pi^+\pi^-\pi^0$ was investigated by the ARGUS collaboration. The reaction is dominated by the formation of the $a_2(1320)$ meson. A value of $\Gamma_{\gamma\gamma} = (0.96 \pm 0.03 \pm 0.13)$ keV was obtained for its radiative width, in good agreement with the world average. The fraction of $\gamma\gamma$-helicity 0 in the a_2 two-photon width was found to be equal to $(6.7 \pm 2.2)\%$. It allows a discrimination among models that describe the dynamics in the two–photon production of tensor mesons. An upper limit of $\Gamma_{\gamma\gamma} \cdot \mathrm{Br}(\rho^{\pm}\pi^{\mp}) < 0.54$ keV (90% c.l.) was obtained for the resonance $\pi(1300)$. The partial wave analysis revealed almost a complete absence of the wave with spin and parity $J^P = 2^-$. We also observe no significant enhancement in the $\pi^+\pi^-\pi^0$ invariant mass spectrum that could be attributed to the two-photon production of the $\pi_2(1670)$. The obtained upper limit $\Gamma_{\gamma\gamma}(\pi_2(1670)) < 0.19$ keV at the 90% confidence level is in contradiction with two previous observations.

1 Introduction

Electromagnetic interactions provide an important tool for the investigation of hadronic states. In particular, two–photon decay widths $\Gamma_{\gamma\gamma}$ are related to the flavour content of $q\bar{q}$ states. It is also expected that glueball states or admixtures of glueball states should result in smaller values of $\Gamma_{\gamma\gamma}$. In a gamma–gamma interaction with almost real photons only states with certain quantum numbers are populated which simplifies the determination of spins and parities of the produced states.

It is known that the process $\gamma\gamma \rightarrow \pi^+\pi^-\pi^0$ is dominated by the production of $a_2(1320)$. It has also been observed that the main contribution comes from the helicity 2 amplitude [1, 2, 3, 4]. This is in agreement with expectations that the fraction of the $\gamma\gamma$ helicity zero partial width $r^{(0)} = \Gamma_{\gamma\gamma\,J=2}^{J_z=0} / (\Gamma_{\gamma\gamma\,J=2}^{J_z=0} + \Gamma_{\gamma\gamma\,J=2}^{J_z=2})$ should be small. The predictions for this ratio [5, 6, 7, 8] vary from 0 to $\frac{1}{7}$. A precise experimental determination of the a_2 polarization in two–photon reactions is, therefore, important for selecting models that consistently describe the dynamics of the coupling of a meson to two real photons.

Recently [3, 9], a structure was found above the $a_2(1320)$ and has been identified as $\pi_2(1670)$. A partial wave analysis is necessary in order to establish its quantum numbers and to determine its two–photon decay width. The present study focuses on these two subjects.

2 Data selection and background estimation

The ARGUS detector and details about its trigger and its particle identification capabilities are described elsewhere [10]. The two–photon reaction $\gamma\gamma \rightarrow \pi^+\pi^-\pi^0$ is realised in the DORIS II e^+e^- storage ring via the production process $e^+e^- \rightarrow e^+e^-\gamma\gamma \rightarrow e^+e^-\pi^+\pi^-\pi^0$. Since the final–state electron and positron scatter predominantly along the beam pipe and escape detection (no-tag condition), we require the final–state particles $\pi^+\pi^-\pi^0$ to have a sum of transverse momenta $\sum \vec{p}_T$ close to zero and that no other particles be detected. In this way only events corresponding to almost real photons are selected. The data used for the study of this reaction were taken at an

average e^+e^- centre–of–mass energy of 10.4 GeV and correspond to an integrated luminosity of Λ =456 pb^{-1}.

The selected events consisted of two charged tracks and two photon signals. The tracks had to have opposite sign and to originate from a common vertex at the beam line. Only tracks that had a likelihood for being pions [10] above 1% and a likelihood for being electrons and muons [10] less than 10% were considered. Calorimeter noise was kept low by requiring a minimum photon energy of 70 MeV. A more serious fake photon background arises, however, when showers resulting from the impact of charged particles become split and the resulting calorimeter pattern is misinterpreted as being due to two closely spaced hits. In order not to consider them as real photons, a cut was applied on the angle α between the photon direction and the line connecting the vertex with the impact point of the charged pion in the calorimeter. Only hits with $\cos\alpha < 0.9$ were identified as photons. A π^0 candidate was formed by combining two photons with an opening angle below 90°. In order to be accepted as a π^0, the invariant mass of a candidate had to lie between 60 and 210 MeV/c^2. Its mass was constrained to the nominal π^0 mass value by adjusting the photon momenta. A cut on the scalar momentum of the three pions $\sum_i |\vec{p}_i| \leq 4$ GeV/c and a cut on the total transverse momentum $|\sum_i \vec{p}_{T,i}| \leq 120$ MeV/c were used to enhance two–photon interactions and to suppress the background from τ decays and incompletely reconstructed events. The background from $\gamma\gamma \to \pi^+\pi^-$ and $\gamma\gamma \to \mu^+\mu^-(e^+e^-)$ with additional noise in the calorimeter was diminished by applying a cut on the sum of the transverse momenta of the two charged pions, $|\vec{p}_T(\pi^+) + \vec{p}_T(\pi^-)|^2 > 0.004$ GeV^2/c^2. After imposing these selection criteria, 3567 events remained. Their invariant mass spectrum is shown in figure 1. The three-pion invariant mass distribution of the selected sample clearly peaks at the position of the $a_2(1320)$ resonance. The experimental resolution of the three–pion invariant mass and the pion angular distributions is dominated by the π^0 momentum resolution. We compensate for this by adjusting the π^0 transverse momentum so that the total transverse momentum of the three pions equals to zero:

$$\vec{p_T}(\pi^0) \to \vec{p_T}^*(\pi^0) = -(\vec{p_T}(\pi^+) + \vec{p_T}(\pi^-)) \; . \tag{1}$$

The rationale behind this momentum tuning is that the final state transverse momentum is dominantly very small since events are collisions of almost real bremsstrahlung from the incident e^+e^-.

The background contribution was obtained from a Monte Carlo simulation using an event generator based on measured cross sections. The largest contribution to the background comes from $\gamma\gamma \to \pi^+\pi^-\pi^0\pi^0$ with one π^0 undetected. It amounts to 200 events as obtained from the measured cross section [11]. A significant contribution of 150 events originates from $\gamma\gamma \to \pi^+\pi^-\pi^0$ where a photon from the π^0 is lost and replaced by a noise signal in the calorimeter. The reaction $\gamma\gamma \to \eta' \to \rho^0\gamma \to \pi^+\pi^-\gamma$ [12] can also simulate a $\gamma\gamma \to \pi^+\pi^-\pi^0$ signal when combined with calorimeter noise. This background was estimated to be about 23 events. The contribution from $e^+e^- \to \tau^+\tau^-$ amounts to less than 10 events, while the background resulting from $e^+e^- \to q\bar{q}$ and $e^+e^- \to B\bar{B}$ can be neglected. To reduce the contribution from events originating from the interaction of primary electrons and positrons with the beam–pipe gas and walls, cuts on the origin of tracks were applied which brought this kind of background contamination to less than 35 events. In total, the contribution from the various backgrounds to the selected sample is estimated to be 12%.

3 Analysis of the $\pi^+\pi^-\pi^0$ final state

The experimental data were analysed by using a maximum likelihood method [13]. A likelihood function was defined as

$$\ln L = \sum_{i=1}^{N} \ln \left\{ \sum_{k,l} P_{k,l} \lambda_k \lambda_l \frac{A_k(\xi_i)}{\sqrt{|A_k|^2}} \frac{A_l^*(\xi_i)}{\sqrt{|A_l|^2}} \right\} - N S, \tag{2}$$

where the first summation extends over all measured events i. The meaning of the symbols is as follows.

$A_k(\xi)$**:** A transition amplitude for the decay channel k that depends on measured variables (invariant masses and angles) which are symbolically denoted by ξ. Apart from terms, containing the final state invariant mass $W_{\gamma\gamma}$, the transition amplitude for the decay of a state with spin and parity J^P via an isobar I reads

$$A_k \propto B((J^P, J_z) \to I\pi;\ I \to \pi\pi) f(I \to \pi\pi) RBW(I)\,, \tag{3}$$

where the $\gamma\gamma$-helicity J_z is defined as a component of the spin J along the direction of the incoming photons in the three–pion center-of-mass system. The relativistic Breit-Wigner function

$$RBW(I) = \frac{1}{m_I^2 - m_{(\pi\pi)_I}^2 - i m_I \Gamma_I} \tag{4}$$

represents the propagator of the isobar I, decaying into two pions. The symbol $m_{(\pi\pi)_I}$ stands for the invariant mass of the two pions which combine into the isobar I while m_I and Γ_I are nominal mass and full width of the isobar. The angular dependence (see figure 2 for the definition of angles) is described by the amplitudes

$$\begin{aligned} &B_L((J^P, J_z) \to I\pi;\ I \to \pi\pi) = \\ &p_I^L p_\pi^j \sum_{j_z(I)+M=J_z} C^{J,J_z}_{j(I),j_z(I),L,M} Y_L^M(\theta(I), \phi(I)) Y_j^m(\theta_1(\pi_I), \phi_1(\pi_I))\,, \end{aligned} \tag{5}$$

written in terms of momenta, spherical harmonics and appropriate Clebsch-Gordon coefficients. The latter combine the orbital angular momenta $\vec{L}$ of isobars with their spins $\vec{j}$ to the overall angular momenta $\vec{J}$ of different partial waves. The momentum p_I of the isobar I is calculated in the $\pi^+\pi^-\pi^0$ rest frame and p_π is the pion momentum in the isobar center-of-mass system.

The form factors $f(I \to \pi\pi)$ are smoothly varying scalar functions of masses of the involved particles. For the decay $\rho \to \pi\pi$ we took a form factor proposed in [14], for the transition $f_2 \to \pi\pi$ we used slightly modified Blatt-Weisskopf form factors [15, 13] while form factor for the decay of the narrow $f_0(980)$ was assumed to be constant.

Note that the large width of the ρ makes the interference terms between $(J^P, J_z) \to \rho^+\pi^-$ and $(J^P, J_z) \to \rho^-\pi^+$ decays non negligible. This means that every transition amplitude

for the decay through $\rho\pi$ must be written as a sum of the amplitudes for the two decay channels [5]

$$A_k((J^P, J_z) \to \rho\pi;\ \rho \to \pi\pi) = \\ A_k((J^P, J_z) \to \rho^+\pi^-; \rho^+ \to \pi^+\pi^0) + A_k((J^P, J_z) \to \rho^-\pi^+; \rho^- \to \pi^-\pi^0)\ . \tag{6}$$

$P_{k,l} = e^{i\delta_{kl}}$**:** Elements of a Hermitian matrix. All diagonal elements are equal to 1. The off-diagonal elements differ from zero only when interference between states k and l is possible. δ_{kl} is a relative phase between A_k and A_l.

$\overline{|A_k|^2}$**:** A normalization factor defined as an integral of $|A_k(\xi)|^2$ over the variables ξ weighted by the acceptance $\eta_k(W_{\gamma\gamma})$, the two–photon luminosity function $dL_{\gamma\gamma}/dW_{\gamma\gamma}$ and the phase space density. It is obtained from a Monte Carlo simulation of the detector performance.

λ_k^2**:** Fractions of the measured events that are attributed to particular partial waves k. They are obtained by requiring a maximum value of the likelihood function L.

S**:** Normalization integral,

$$S = \sum_{k,l} P_{k,l}\lambda_k\lambda_l \frac{\overline{A_k A_l^*}}{\sqrt{\overline{|A_k|^2}}\sqrt{\overline{|A_l|^2}}}. \tag{7}$$

The partial wave analysis was performed for each of the 50 MeV/c^2 final–state invariant mass intervals separately. Altogether the following partial waves were taken into account:

$$\begin{array}{lcl} (2^+,+2) & \to & \rho^\pm\pi^\mp \\ (2^+,-2) & \to & \rho^\pm\pi^\mp \\ (2^+,0) & \to & \rho^\pm\pi^\mp \\ (2^+,2) & \to & f_2\pi^0 \\ (2^+,0) & \to & f_2\pi^0 \\ (2^-,0) & \to & \rho^\pm\pi^\mp \\ (2^-,0) & \to & f_2\pi^0 \\ (0^-,0) & \to & \rho^\pm\pi^\mp \\ (0^-,0) & \to & f_2\pi^0 \\ (0^-,0) & \to & f_0\pi^0 \\ \text{isotropic} & \to & \pi^+\pi^-\pi^0, \end{array}$$

where $(2^+,0)$ etc. stand for (J^P, J_z). By "isotropic" we mean the fraction which is assumed to be distributed isotropically in phase space.

Note that $\gamma\gamma \to a_2$ involves only the first three waves. Since the resonance $a_2(1320)$ dominates the three–pion invariant masses below 1.45 GeV/c^2 (see figure 1), the analysis was divided into two parts which cover the mass regions 0.8 – 1.45 GeV/c^2 and 1.45 – 2.1 GeV/c^2. In the low–mass region the fractions λ_k^2 of only five channels were varied:

$$\begin{array}{lcl} (2^+,+2) & \to & \rho^\pm\pi^\mp \\ (2^+,-2) & \to & \rho^\pm\pi^\mp \end{array}$$

$$
\begin{array}{lcl}
(2^+,0) & \rightarrow & \rho^{\pm}\pi^{\mp} \\
(0^-,0) & \rightarrow & \rho^{\pm}\pi^{\mp} \\
\text{isotropic} & \rightarrow & \pi^+\pi^-\pi^0,
\end{array}
$$

The radially excited $J^P = 2^-$ states are not expected to appear in this mass region, and states decaying into $f_2\pi^0$ are suppressed due to the high threshold.

The high–mass region (from 1.45 to 2.1 GeV/c^2), on the other hand, is characterized by small numbers of events per bin (typically 70, see figure 1). In order to obtain stable results from the maximum likelihood analysis, the number of variables had to be kept low. Results of the analysis in the low–mass region show that the helicity 0 wave $(2^+,0) \rightarrow \rho^{\pm}\pi^{\mp}$ is suppressed (see section 4), therefore we consider both $(2^+,0) \rightarrow \rho^{\pm}\pi^{\mp}$ and $(2^+,0) \rightarrow f_2\pi^0$ fractions in the high–mass region to be negligible and they are therefore set to 0. Figure 6.d shows the $\pi^+\pi^-$ invariant mass spectrum for the three–pion invariant mass interval between 1.45 and 1.90 GeV/c^2. The main peak in the distribution could be interpreted as the $f_2(1270)$ resonance. The observed shift of about 70 MeV/^{2} towards smaller masses can be explained by the phase space suppression. The lowest $f_2\pi^0$ waves are the s-wave with the spin-parity and $\gamma\gamma$-helicity $(J^P, J_z) = (2^-,0)$, p-wave with $(2^+,2)$ and d-waves with $(0^-,0)$ and $(2^-,0)$. First, the analysis was performed with the inclusion of all above waves regardless to the low statistics. A stable solution was obtained for 11 out of 13 $W_{\gamma\gamma}$ intervals of 50 MeV/c^2 width. In all of them the number of d-wave $f_2\pi$ events was found to be consistent with zero. Therefore, we omitted the highest orbital momentum $f_2\pi$ channels from the final analysis, particularly since we do not expect a considerable $L = 2$ contribution so close to the threshold for the $f_2\pi^0$ production. The additional peak that is seen in the $\pi^+\pi^-$ spectrum (fig. 6.d) is attributed to $f_0(980)$. The corresponding $f_0\pi^0$ contribution to the integrated $\gamma\gamma \rightarrow \pi^+\pi^-\pi^0$ cross section is less than 5%, therefore only the s-wave was included in the maximum likelihood function. To summarize, in the final analysis of the high–mass region we varied fractions of channels

$$
\begin{array}{lcl}
(2^+,2) & \rightarrow & \rho^{\pm}\pi^{\mp} \\
(2^+,2) & \rightarrow & f_2\pi^0 \\
(2^-,0) & \rightarrow & \rho^{\pm}\pi^{\mp} \\
(2^-,0) & \rightarrow & f_2\pi^0 \\
(0^-,0) & \rightarrow & \rho^{\pm}\pi^{\mp} \\
(0^-,0) & \rightarrow & f_0\pi^0 \\
\text{isotropic} & \rightarrow & \pi^+\pi^-\pi^0\,.
\end{array}
$$

4 Determination of resonance parameters and cross sections

The low–mass region (events with the three–pion invariant mass between 0.8 and 1.45 GeV/c^2), apart from being dominated by $(2^+, \pm 2)$ from $a_2(1320)$, also shows a small contribution from $(0^-,0) \rightarrow \rho^{\pm}\pi^{\mp}$ (presumably $\pi(1300)$) and the isotropic channel. The results of the maximum likelihood fit are shown in figure 3.

In order to extract the value for the product of branching ratios and two–photon partial width of the $a_2(1320)$, the measured invariant mass distributions of the $2^+ \rightarrow \rho^{\pm}\pi^{\mp}$ waves were fitted

to a resonance function which consisted of a relativistic Breit–Wigner function multiplied by the two–photon luminosity function, acceptance corrected and convoluted with a Gaussian distribution to account for the experimental resolution. The corresponding fit curves are also shown in figure 3. Using the PDG [16] branching ratios for $a_2 \to \rho\pi$ and $\rho \to \pi\pi$, a value of

$$\Gamma_{\gamma\gamma}(a_2(1320)) = (0.96 \pm 0.03 \pm 0.13)\ \mathrm{keV} \tag{8}$$

was obtained for the radiative partial width $\Gamma_{\gamma\gamma}(a_2)$.[1] The other two resonance parameters obtained from the fit

$$m(a_2) = 1320 \pm 7\ \mathrm{MeV/c^2} \tag{9}$$

$$\Gamma(a_2) = 120 \pm 20\ \mathrm{MeV} \tag{10}$$

are consistent with the PDG [16] values. The relative contribution of $\Gamma_{\gamma\gamma}(J_z = 0)$ to the a_2 two–photon width amounts to

$$r^{(0)} = (6.7 \pm 2.2)\% \ . \tag{11}$$

The correlation coefficient between the two $\gamma\gamma$-helicity amplitudes is nonzero which had to be taken into account in the determination of the statistical error on $r^{(0)}$.

We observed only a small contribution from the $(0^-, 0) \to \rho^{\pm}\pi^{\mp}$ wave with no clear indication of an excess of events near the $\pi(1300)$ nominal mass [16] (see figure 3). We converted the resulting number of candidates (109 ± 27) in the three–pion invariant mass interval between 1.1 and 1.5 GeV/c^2 into an upper limit for a product of the $\pi(1300)$ two-photon width and its branching ratio for the decay into $\rho\pi$:

$$\Gamma_{\gamma\gamma}(\pi(1300)) \times \mathrm{BR}(\pi(1300) \to \rho^{\pm}\pi^{\mp}) < 0.54\ \mathrm{keV}\ (90\%\ \mathrm{conf.\ level}). \tag{12}$$

The full width and the nominal mass of the resonance were assumed to take values within one standard deviation from the average values of previous $\pi(1300)$ observations [16].

Contrary to expectations, based on previous measurements [9, 3], the obtained fractions of the $(2^-, 0) \to \rho\pi$ and $(2^-, 0) \to f_2\pi$ channels in the high–mass interval are small and show *no* significant enhancements in the $\pi_2(1670)$ region (fig. 4). In the interval between $W_{\gamma\gamma 1} = 1500$ MeV/c^2 and $W_{\gamma\gamma 2} = 1800$ MeV/c^2, we attributed 15.1 ± 19.7 and 14.4 ± 12.5 events to the $(2^-, 0) \to \rho\pi$ and $(2^-, 0) \to f_2\pi$ channels, respectively. If we assume that these values are uncorrelated, the two numbers combined with the systematic uncertainties (see section 5 and table 3) give

$$\Gamma_{\gamma\gamma}(\pi_2(1670)) < 0.19\ \mathrm{keV}\ (90\%\ \mathrm{c.l.})\ . \tag{13}$$

Note that the obtained limit is in contradiction with the $\Gamma_{\gamma\gamma}(\pi_2(1670))$ values, measured by the Crystal Ball [9] and CELLO [3] collaborations. The reason for the discrepancy is extensively searched for in the next section.

The total cross section for the reaction $\gamma\gamma \to \pi^+\pi^-\pi^0$ is shown in figure 5 and the cross sections for the partial waves k are listed in tables 1 and 2. They were obtained by averaging

[1] Whenever two errors are quoted the first applies to the statistical and the second to the systematic errors.

over 50 MeV/c^2 wide $W_{\gamma\gamma}$ bins using the following formula:

$$\sigma_{\gamma\gamma\to k} = \frac{N_k(W_{\gamma\gamma})}{\eta_k} \frac{1}{\Lambda \frac{dL_{\gamma\gamma}}{dW_{\gamma\gamma}} \Delta W_{\gamma\gamma}} , \tag{14}$$

where

$$N_k(W_{\gamma\gamma}) = N(W_{\gamma\gamma})\lambda_k^2 - N_k^{\rm bck}(W_{\gamma\gamma}) \tag{15}$$

is the background subtracted number of events with the three–pion invariant mass between $W_{\gamma\gamma} - \frac{\Delta W_{\gamma\gamma}}{2}$ and $W_{\gamma\gamma} + \frac{\Delta W_{\gamma\gamma}}{2}$, attributed to the channel k. $N_k^{\rm bck}(W_{\gamma\gamma})$ is the number of background events in the same channel, obtained by the MC simulation (see also section 5), while $N(W_{\gamma\gamma})$ is the number of all selected $\pi^+\pi^-\pi^0$ events in the appropriate $W_{\gamma\gamma}$ interval. Acceptances η_k for the partial waves, determined by the simulation of the detector performance, are of the order of few percents and vary smoothly with the three-pion invariant mass. Note that the errors quoted in the tables 1 and 2 are statistical only and do not include the systematic uncertainties of the acceptance determination.

5 Estimation of systematic uncertainties

A major part of the analysis was devoted to the study of systematic errors. In what follows, some of the aspects involved are discussed.

In order to check the acceptance for photons that was calculated from the Monte Carlo simulation of the calorimeter, an independent analysis was performed, making use of events where only one final–state photon in the reaction $\gamma\gamma \to \pi^+\pi^-\pi^0 \to \pi^+\pi^- 2\gamma$ was detected[2]. To this photon a mass was attributed that was equal to the π^0 mass. The photon momentum was readjusted to obtain a minimal value for $\sum \vec{p}_T$. In addition, a kinematical criterion was introduced in order to suppress $\gamma\gamma \to \eta' \to \rho^0\gamma \to \pi^+\pi^-\gamma$ events. It removed events outside a circle of radius 250 MeV/c^2 around the ρ mass value in a two-dimensional $\pi^+\pi^0$ vs. $\pi^-\pi^0$ invariant mass space. The analysis was then performed in a manner similar to the case with two detected photons, and the measured and simulated ratios of one–photon to two–photon events were found to be equal within the statistical errors.

The reaction $\gamma\gamma \to \eta' \to \pi^+\pi^-\gamma$ itself is interesting from the point of view of the trigger efficiency determination. The triggering of that reaction is done by the charged pions in the final state [10], therefore it is expected to be very similar to the triggering of our reaction $\gamma\gamma \to \pi^+\pi^-\pi^0$. The two-photon width of η', measured by ARGUS experiment [12] is in a perfect agreement with the world average [16]. This is an indication that the program, used to determine the trigger efficiency, properly simulates the real trigger conditions. The simulated trigger efficiencies have also been compared to trigger efficiencies deduced directly from the data, using the transition $\Upsilon(2S) \to \Upsilon(1S)\pi^+\pi^-$ [10]. The two trigger efficiencies were consistent within the statistical errors of the limited $\Upsilon(2S)$ data sample.

The dependence of the results on the choice of the initial photon form factors was checked by varying them from a constant value to a ρ–pole form factor. This resulted in a 3% contribution

[2] Note that such events were used to obtain the first measured value for $\Gamma_{\gamma\gamma}(a_2)$ [17].

to the systematic error of the two–photon widths. The effect of variation of the parameters in the Breit–Wigner formula was also tested. In particular, by choosing different parametrizations of the momentum dependent $a_2(1320)$ width we obtained a 5% effect on the extracted value of $\Gamma_{\gamma\gamma}(a_2)$. Taking different expressions for the form factors in the transition amplitudes A_k had, on the other hand, no sizeable impact on the results of the partial wave analysis. Similarly, the effect of different event selection criteria on the fractions λ_k^2 was found to be only 2% and thus negligible.

The maximum likelihood analysis was extensively tested on Monte Carlo generated events. Samples of different (J^P, J_z) and isobar composition were generated and analysed in the same way as the measured data. In all cases the input data were correctly reproduced.

In order to verify the presence of $\rho^{\pm}$ and f_2 in the final state, the measured two–particle invariant mass distributions were compared to the results of the partial wave analysis (fig. 6). The agreement is good within the statistical accuracy. Angular distributions, shown in figures 7 and 8, are strongly affected by the detector acceptance. Nevertheless, we can use them to at least qualitatively distinguish between the various partial waves. For example, the measured distribution of $\cos\theta(\rho^{\pm})$ (fig. 7) clearly prefers the $\gamma\gamma$-helicity 2 component of the $J^P(\rho\pi) = 2^+$ wave to the $\gamma\gamma$-helicity 0 component.

A major source of uncertainty in the determination of $\Gamma_{\gamma\gamma}(\pi_2(1670))$ could come from the interference between the decays of an intermediate $(2^-, 0)$ state into $\rho\pi$ and $f_2\pi$ [3]. The available number of events did not allow for a direct determination of the relative phase. Instead of that, the contribution to the overall systematic error was estimated by performing a threefold analysis of the data, assuming incoherent $f_2\pi^0$ and $\rho^{\pm}\pi^{\mp}$ decay modes, a coherent addition of $f_2\pi^0$ and $\rho^{\pm}\pi^{\mp}$, or a coherent subtraction of the two.

The effect of background sources on the partial wave analysis was checked by simulating the two main sources of background. In the case of $\gamma\gamma \to \pi^+\pi^-\pi^0\pi^0$ with two photons undetected, almost the entire background migrated to the isotropic channel. This is conceivable because through the loss of two photons the correlations in the $\rho^+\rho^-$ channel become weak. The second most important background resulting from the channel $\gamma\gamma \to \pi^+\pi^-\pi^0$ where one photon is lost and replaced by a calorimeter noise hit, does not cause problems in the analysis. Such events behave very much like the unaffected $\gamma\gamma \to \pi^+\pi^-\pi^0$ signals. Again, this is to be expected since the energy of the lost photon is most likely low, and information about the π^0 momentum is carried mainly by the detected photon. Other sources of background are too weak to have any effect on the results.

The contributions from the main sources of systematic errors are listed in table 3.

At the end of section 4 we stressed that our upper limit on $\Gamma_{\gamma\gamma}(\pi_2(1670))$ contradicts results of the two previous measurements. Searching for the reason of the disagreement between their and our observations we repeated the analysis roughly following the method of the CELLO collaboration [3] which also analysed the $\pi^+\pi^-\pi^0$ channel. We extrapolated the contribution of the $(2^+, 2) \to \rho\pi$ wave from the low–mass interval as it is indicated by the dotted line in figure 3. We varied the fractions

$$(2^-, 0) \quad \to \quad \rho^{\pm}\pi^{\mp}$$

$$
\begin{array}{lcl}
(2^-,0) & \rightarrow & f_2\pi^0 \\
\text{isotropic} & \rightarrow & \pi^+\pi^-\pi^0,
\end{array}
$$

while all other waves were excluded from the likelihood method in this reduced model. Upper limits, obtained with the reduced model range from 0.55 to 0.91 keV (table 4), depending on which of the two decay channels we used and what was the assumed interference between the channels. These values are still lower than the values, extracted from the two previously published observations [16]. The CELLO collaboration, for example, obtained $\Gamma_{\gamma\gamma}(\pi_2(1670)) = 1.3 \pm 0.3 \pm 0.12$ keV for the incoherent addition of the $\rho\pi$ and $f_2\pi$ amplitudes, $\Gamma_{\gamma\gamma}(\pi_2(1670)) = 0.8 \pm 0.3 \pm 0.12$ keV for the coherent addition and $\Gamma_{\gamma\gamma}(\pi_2(1670)) = 1.5 \pm 0.5 \pm 0.12$ keV for the coherent subtraction.

Furthermore, we found no good reason to use the reduced model. The likelihood function increases significantly if we vary all the fractions as described in section 3. For example, the one–dimensional angular distributions in figure 8 show that the reduced model describes the data significantly worse than the full model: the χ^2 for the distribution obtained by the full model analysis is 31.6 per 20 degrees of freedom, while the χ^2's for the reduced model distributions range from 39.2 to 51.3. In addition, the full model was always able to correctly reproduce simulated mixtures of different partial waves. Therefore we exclude the possibility that a significant $\pi_2(1670)$ signal in the data could have been assigned to the wrong partial waves in the results of the maximum likelihood method.

6 Conclusion

We performed a partial wave analysis of the reaction $\gamma\gamma \rightarrow \pi^+\pi^-\pi^0$. Using a maximum likelihood method we obtained a value $\Gamma_{\gamma\gamma}(a_2(1320)) = 0.96 \pm 0.03(\mathrm{stat}) \pm 0.13(\mathrm{syst})$ keV for the radiative width of the tensor meson $a_2(1320)$. This confirms the former world average with a precision, comparable to the error on the combination of all previous results.

We also measured the spin alignment of a_2 mesons, produced in two-photon reactions. The value $r^{(0)} = \Gamma_{\gamma\gamma\,J=2}^{J_z=0}/(\Gamma_{\gamma\gamma\,J=2}^{J_z=0} + \Gamma_{\gamma\gamma\,J=2}^{J_z=2}) = (6.7 \pm 2.2)\%$ made it possible to distinguish between different dynamical models for the coupling of a tensor meson to two real photons. Static quark model pictures [5] predict a $\gamma\gamma$-helicity ratio $r^{(0)} = 1/7 = 14.3\%$. If one assumes that only the lowest multipole in the two–photon multipole contributes to the tensor–meson formation, the same prediction for the $r^{(0)}$ is obtained just by the Clebsch–Gordan coefficients that combine two $(J^P, J_z) = (1^-, \pm 1)$ particles to the states with $(2^+, \pm 2)$ and $(2^+, 0)$ [5, 6]. Such a value is now excluded at a level of more than 3.4 standard deviations. Similarly, predictions using the nonrelativistic quark model [7] and the Grassberger-Kögerler sum rule [8] ($r^{(0)} \approx 0$) can be excluded at a level of more than 3 standard deviations. The relativistic $q\overline{q}$ bound state calculation, which predicts $r^{(0)} \leq 6\%$ [7], is, on the other hand, consistent with our measurement.

We found no evidence for the two-photon formation of a pseudoscalar $\pi(1300)$ and give an upper limit $\Gamma_{\gamma\gamma}(\pi(1300)) \times BR(\pi(1300) \rightarrow \rho\pi) \leq 0.54$ keV (90% c.l.).

Contrary to the results of the Crystal Ball and CELLO experiments [9, 3], we observed no significant enhancement in the $\pi^+\pi^-\pi^0$ invariant mass spectrum which could be attributed to the two-photon formation of $\pi_2(1670)$. Furthermore, the partial wave analysis of the measured

sample revealed almost a complete absence of events with spin and parity $J^P = 2^-$. By assigning the full $(2^-, 0) \to \rho\pi$ and $(2^-, 0) \to f_2\pi$ waves in the three–pion invariant mass between 1500 and 1800 MeV/c^2 to the production of the $\pi_2(1670)$, an upper limit of $\Gamma_{\gamma\gamma}(\pi_2(1670)) < 0.19$ keV $(90\%$ c.l.$)$ is obtained for the two-photon width of this resonance.

The upper limit is in contradiction with the previous observations. An important part of the analysis was devoted to the investigation of systematic errors which could be the reason for the discrepancy. The estimated uncertainties are by far too small to accommodate our findings with the surprisingly high results of the two previous experiments [18, 19].

Acknowledgement
It is a pleasure to thank U. Djuanda, E. Konrad, E. Michel, and W. Reinsch for their competent technical help in running the experiment and processing the data. We thank Dr. H. Nesemann, B. Sarau, and the DORIS group for the excellent operation of the storage ring. The visiting groups wish to thank the DESY directorate for the support and kind hospitality extended to them.

References

[1] PLUTO Collab., Ch. Berger et al., Phys.Lett. **249B**, (1984) 427.

[2] CRYSTAL BALL Collab., D. Antreasyan et al., Phys. Rev. **D33**, (1986) 1847.

[3] CELLO Collab., H. J. Behrend et al., Z. Phys. **C46**, (1990) 583.

[4] A.R. Barker, TPC/2γ Collab., Ph.D. Thesis, University of California, Santa Barbara, 1988.

[5] M. Poppe, Int. J. Mod. Phys. **1** (1986) 545.

[6] H. Kolanoski, *Two–Photon Physics at e^+e^- Storage Rings*, Springer–Verlag, 1984.

[7] Z.P. Li, F.E. Close and T. Barnes, Phys. Rev. **D43** (1991) 2161.

[8] P. Grassberger, P. Kögerler, Nucl. Phys. **106B** (1976) 451.

[9] CRYSTAL BALL Collab., D. Antreasyan et al., Z. Phys. **C48**, (1990) 561.

[10] ARGUS Collab., H.Albrecht et al., Nucl.Instrum.Methods, **A275**, (1989) 1.

[11] ARGUS Collab., H.Albrecht et al., Phys.Lett. **217B**, (1991) 205.

[12] K.W. McLean, *$\pi^+\pi^-\gamma$ and K^+K^- Production in Two Photon Collisions at ARGUS*, Ph.D. Thesis McGill University, Montreal, Canada (1990).

[13] T. Podobnik, *Resonances Observed in the Reaction $\gamma\gamma \to \pi^+\pi^-\pi^0$*, Doctoral thesis, Univerza v Ljubljani, 1995.

[14] J.D.Jackson, Nuovo Cimento **34** (1964) 1644.

[15] J.M.Blatt,V.Weisskopf, *Theoretical Nuclear Physics*, John Wiley, New York, 1952.

[16] Particle Data Group, Review of Particle Properties, Phys. Rev. **D50** (1994) 1173.

[17] CELLO Collab., H.J. Behrend et al., Phys.Lett. **114B**, (1982) 378.

[18] J.D.Anderson, M.H.Austern, R.N.Cahn, Phys.Rev. **D 43** (1991) 2094.

[19] E.S.Ackleh, T.Barnes, Phys.Rev. **D 45** (1992)232.

$W_{\gamma\gamma}$ [MeV/c^2]	$(2^+,2) \to \rho\pi$	$(2^+,0) \to \rho\pi$	$(0^-,0) \to \rho\pi$	isotr. $\pi^+\pi^-\pi^0$	$\sum$
$800-850$	-1.2 ± 2.1	0.1 ± 2.0	-0.1 ± 1.3	20.9 ± 3.4	19.6 ± 3.9
$850-900$	2.2 ± 2.7	1.7 ± 2.0	5.6 ± 5.9	6.1 ± 1.0	15.5 ± 4.1
$900-950$	3.5 ± 3.4	-1.6 ± 2.4	5.4 ± 7.1	15.2 ± 2.0	22.5 ± 4.5
$950-1000$	0.0 ± 3.7	-1.8 ± 1.5	0.5 ± 6.8	27.7 ± 3.2	26.4 ± 4.7
$1000-1050$	-0.7 ± 2.5	0.0 ± 1.6	0.9 ± 5.1	23.6 ± 2.8	23.7 ± 4.1
$1050-1100$	9.6 ± 2.9	0.2 ± 1.2	6.4 ± 2.8	2.7 ± 3.8	19.0 ± 3.4
$1100-1150$	13.7 ± 3.4	-2.7 ± 1.3	5.5 ± 2.7	10.6 ± 4.1	27.0 ± 4.0
$1150-1200$	13.3 ± 3.4	3.1 ± 2.0	7.7 ± 2.9	5.3 ± 3.5	29.4 ± 4.1
$1200-1250$	41.6 ± 5.8	0.3 ± 2.9	2.3 ± 3.2	21.1 ± 5.6	65.2 ± 6.1
$1250-1300$	97.4 ± 8.7	2.3 ± 4.2	5.1 ± 4.4	15.0 ± 5.4	119.8 ± 8.3
$1300-1350$	128.1 ± 9.9	14.4 ± 4.9	4.7 ± 4.8	5.1 ± 5.0	152.2 ± 9.3
$1350-1400$	80.7 ± 8.0	7.0 ± 4.0	3.8 ± 4.4	12.7 ± 4.7	104.3 ± 7.8
$1400-1450$	35.5 ± 5.5	9.2 ± 3.2	6.5 ± 4.1	14.2 ± 4.5	65.4 ± 6.2

Table 1: Cross sections (in nanobarns) for two-photon production of various partial waves in the 3π invariant mass interval below 1.45 GeV/c^2. Note that the errors shown are statistical only. Also given is the sum of all cross sections for every separate $W_{\gamma\gamma}$ bin. The error of the sum was calculated taking into account the correlations between the fractions of partial waves.

$W_{\gamma\gamma}$ [MeV/c^2]	$(2^+,2) \to \rho\pi$	$(0^-,0) \to \rho\pi$	$(2^-,0) \to \rho\pi$	isotr. $\pi^+\pi^-\pi^0$
$1450-1500$	29.8 ± 6.9	1.8 ± 5.1	3.1 ± 2.1	14.6 ± 2.3
$1500-1550$	22.1 ± 5.3	-0.9 ± 4.1	3.1 ± 4.3	5.0 ± 1.6
$1550-1600$	16.2 ± 4.9	-0.3 ± 4.1	5.5 ± 2.6	3.4 ± 2.3
$1600-1650$	21.8 ± 5.2	2.6 ± 3.4	-10.3 ± 5.8	5.7 ± 2.3
$1650-1700$	4.1 ± 4.0	-3.6 ± 3.8	8.9 ± 4.6	9.8 ± 2.1
$1700-1750$	4.6 ± 3.0	-1.6 ± 2.9	6.1 ± 5.9	8.4 ± 2.0
$1750-1800$	11.2 ± 5.1	6.0 ± 4.1	-4.3 ± 6.3	8.0 ± 2.6
$1800-1850$	5.0 ± 3.9	-2.1 ± 4.1	12.0 ± 6.5	10.0 ± 2.8
$1850-1900$	10.0 ± 4.3	1.2 ± 3.6	-3.3 ± 6.8	12.7 ± 3.6
$1900-1950$	19.2 ± 6.6	4.3 ± 4.2	-12.8 ± 5.8	7.5 ± 1.9
$1950-2000$	5.0 ± 4.2	9.4 ± 3.6	-5.8 ± 4.7	1.8 ± 1.9
$2000-2050$	1.8 ± 4.1	0.8 ± 2.7	0.0 ± 3.8	9.3 ± 2.6
$2050-2100$	4.5 ± 3.7	0.0 ± 2.0	-5.2 ± 3.9	10.9 ± 2.8

$W_{\gamma\gamma}$ [MeV/c^2]	$(2^+,2) \to f_2\pi$; $f_2 \to \pi^+\pi^-$	$(2^-,0) \to f_2\pi$; $f_2 \to \pi^+\pi^-$	$(0^-,0) \to f_0\pi$; $f_0 \to \pi^+\pi^-$	$\sum$
$1450-1500$	4.4 ± 0.3	0.2 ± 2.2	0.27 ± 1.00	53.9 ± 5.8
$1500-1550$	6.2 ± 0.6	2.1 ± 2.4	1.47 ± 1.01	39.0 ± 5.8
$1550-1600$	7.4 ± 0.7	0.5 ± 2.2	1.96 ± 1.20	34.1 ± 5.2
$1600-1650$	7.0 ± 0.7	4.7 ± 1.3	0.37 ± 0.65	31.7 ± 5.6
$1650-1700$	3.8 ± 0.5	2.1 ± 0.7	0.27 ± 0.62	25.2 ± 5.0
$1700-1750$	8.4 ± 1.0	-3.4 ± 1.2	0.53 ± 0.76	23.1 ± 5.6
$1750-1800$	4.4 ± 0.5	2.3 ± 1.2	0.51 ± 0.81	28.1 ± 5.8
$1800-1850$	1.6 ± 0.2	3.6 ± 1.1	0.62 ± 0.78	30.7 ± 6.1
$1850-1900$	-5.8 ± 0.8	9.2 ± 1.7	0.85 ± 0.89	24.7 ± 5.2
$1900-1950$	-5.5 ± 0.8	0.2 ± 0.9	-0.15 ± 0.72	12.8 ± 4.0
$1950-2000$	2.5 ± 0.4	2.3 ± 1.0	0.83 ± 0.73	16.1 ± 4.7
$2000-2050$	-1.2 ± 0.2	5.1 ± 1.1	-0.06 ± 0.43	15.6 ± 4.0
$2050-2100$	0.7 ± 0.1	-1.0 ± 2.2	1.00 ± 1.05	10.9 ± 2.2

Table 2: Cross sections (in nanobarns) for two-photon production of considered partial waves and the total $\gamma\gamma \to \pi^+\pi^-\pi^0$ cross section in the 3π invariant mass interval above 1.45 GeV/c^2. The values are obtained with the assumption that the waves with spin and parity 2^- and 0^- add incoherently and that also the different decay channels of the particular waves, e.g. $(2^-,0) \to \rho\pi$ and $(2^-,0) \to f_2\pi$, do not interfere.

	Estimated value (%)		
	$a_2(1320)$	$\pi_2(1670)$	
		$\rho\pi$	$f_2\pi$
Relative $\rho\pi$–$f_2\pi$ phase	–	5.8	20.0
Branching ratios	4	12.7	5.7
Resonance parametrization	5	5	5
Variation of $\overline{\lvert A_k\rvert^2}$'s	4	10.2	8.2
Detector simulation	5		
Trigger simulation	7		
$\gamma\gamma$-vertex parametrization	5		
Background contribution	3		
Selection criteria	2		
Integrated luminosity Λ	1.8		
$\gamma\gamma$ luminosity function	2		
$\sum$	13	21	25

Table 3: List of estimated systematic errors on measured two-photon width of the $a_2(1320)$ and on upper limits of the $\pi_2(1670)$ radiative width.

Assumed interference between the $\rho\pi$ and $f_2\pi$ channels	Decay channel used to extract the upper limit	Upper limit on $\Gamma_{\gamma\gamma}(\pi_2(1670))$ (90% c.l.)
No interference	$\rho\pi$	0.91 keV
	$f_2\pi$	0.55 keV
Positive interference	$\rho\pi$	0.75 keV
	$f_2\pi$	0.56 keV
Negative interference	$\rho\pi$	0.83 keV
	$f_2\pi$	0.66 keV

Table 4: Upper limits on $\pi_2(1670)$ two-photon width as determined by the reduced model.

Figure Captions

Fig. 1: $\pi^+\pi^-\pi^0$ invariant mass distribution after applying all cuts and after tuning the π^0 momenta (see text). The expected contribution from the $a_2(1320)$ is represented by the dotted curve and was obtained with the PDG [16] average resonance parameters.

Fig. 2: On the definition of the angles θ, ϕ and θ_1, ϕ_1. The z axis of the coordinate systems is pointing along the $\gamma\gamma$ axis in the $\pi^+\pi^-\pi^0$ center of mass. In no-tag reactions this coincides, to a very good approximation, with the beam direction. Since the overall azimuthal angle ϕ is redundant in a no-tag experiment, the ρ^+ was chosen to lie in the $z-x$ plane ($\phi = 0$), while for the other isobars (e.g. ρ^- or f_2) ϕ is the difference between their and ρ^+'s azimuthal angle. Note that for the sake of brevity in the definition of angles we call every $\pi^\pm\pi^0$ combination a $\rho^\pm$ meson and every $\pi^+\pi^-$ combination an f_2 meson.

Fig. 3: Results of the partial wave analysis in the low–mass region. In the case of $J^P = 2^+$ waves the results of fits to resonance functions (see text) are also shown. The mass and width of the resonance were treated as free parameters.

Fig. 4: Results of the partial wave analysis in the $m(3\pi)$ interval between 1.45 and 2.10 GeV/c^2. The fit was performed by assuming no interference between the different channels.

Fig. 5: The total $\gamma\gamma \to \pi^+\pi^-\pi^0$ cross section. The errors shown are statistical only. Note that care had to be taken when adding up different contributions because the errors on the cross sections for particular partial waves in the same $W_{\gamma\gamma}$ bin are correlated.

Fig. 6: Measured $m(\pi\pi)$ distributions (crosses) for the events with 3π invariant mass between 1.05 and 1.45 GeV/c^2 (upper row) or 1.45 and 1.90 GeV/c^2 (lower row). Figures a) and c) display invariant mass distributions of $\pi^\pm\pi^0$ combinations (two entries per event) while figures b) and d) show the distributions for charged pion pairs. Histograms indicate distributions, simulated according to the results of the partial wave analysis of the measured sample.

Fig. 7: Polar angle distribution of the $\pi^\pm\pi^0$ pairs for the part of the selected sample with $1.05\mathrm{GeV/c^2} < m(3\pi) < 1.45\mathrm{GeV/c^2}$ (see figure 2 for the definition of the angle). The data (crosses) are compared to the distribution of the simulated sample (histogram), containing fractions of particular partial waves in proportions, obtained by the maximum likelihood method. Also shown are expected distributions for the $(2^+, 2) \to \rho\pi$ (full line) and $(2^+, 0) \to \rho\pi$ (dotted line) channels as well as for the $\pi^+\pi^-\pi^0$, distributed isotropically in the phase space (dashed line).

Fig. 8: Polar angle distribution of the $\pi^+\pi^-$ pairs for the measured events in the $m(3\pi)$ interval between 1.45 and 1.90 GeV (crosses), and corresponding spectrum for the simulated events, generated according to the results of the maximum likelihood method (histogram) (see also figure 2 for the definition of the angle $\theta(f_2)$). Lines indicate distributions, obtained by the reduced model assuming incoherent $\rho\pi$ and $f_2\pi$ decay channels of the $(2^-, 0)$

wave (full line), a coherent addition (dashed line) or a coherent subtraction (dotted line) of the two.

Figure 1:

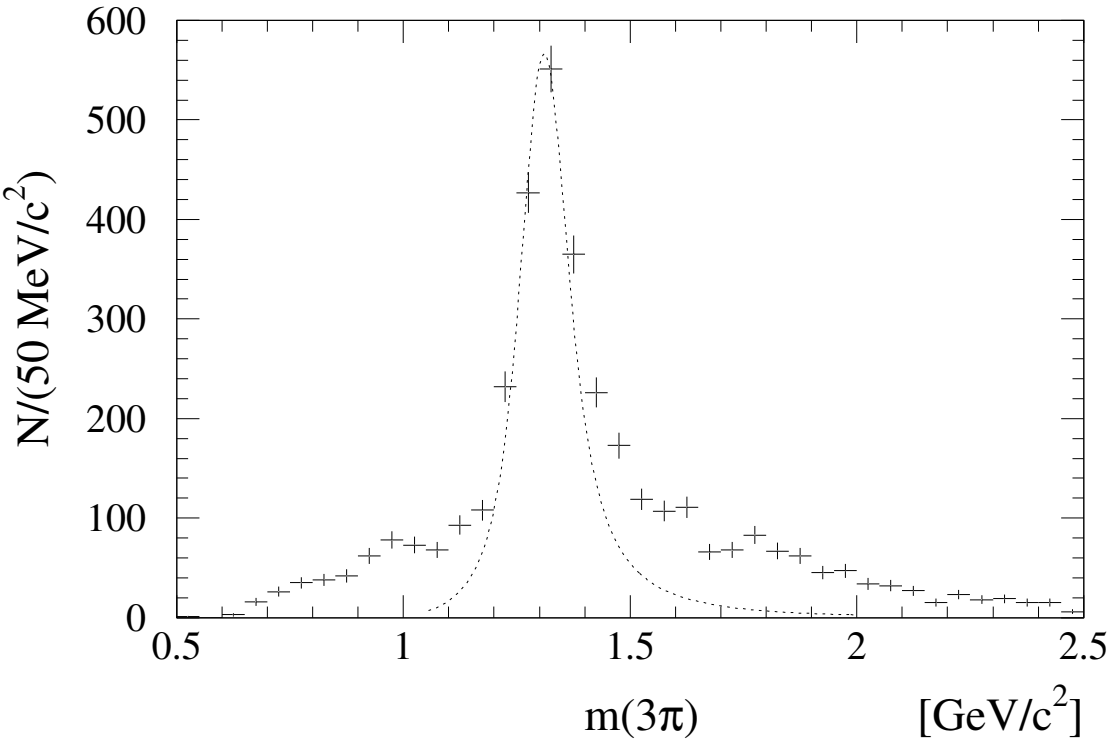
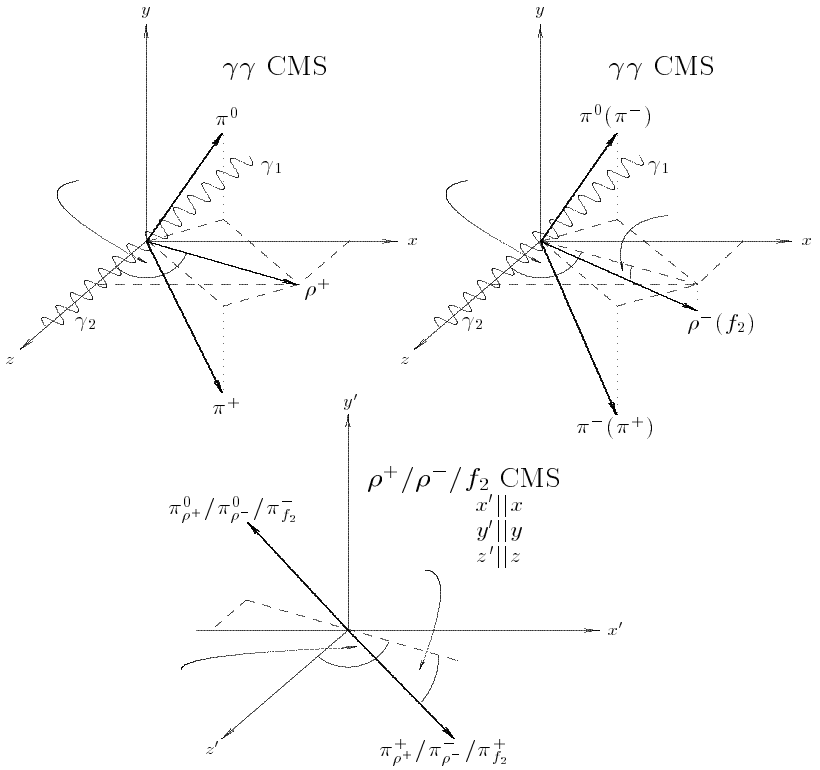
Figure 2: